



Validation of NH₃ observations from AIRS and CrIS against aircraft measurements from DISCOVER-AQ and a surface network in the Magic Valley

5 Karen E. Cady-Pereira¹, Xuehui Guo², Rui Wang³, April B. Leytem⁴, Chase Calkins¹, Elizabeth Berry¹, Kang Sun^{5,6}, Markus Müller⁷, Armin Wisthaler⁷, Vivienne H. Payne⁸, Mark Shephard⁹, Mark Zondlo², Valentin Kantchev^{8,10}

¹ Atmospheric and Environmental Research Inc., Lexington, MA, USA

² Department of Environmental Sciences, University of Virginia, Charlottesville, VA, USA

10 ³ Department of Civil and Environmental Engineering, Princeton University, Princeton, NJ, USA

⁴ United States Department of Agriculture-Agricultural Research Service, Kimberly, ID, USA

⁵ Department of Civil, Structural and Environmental Engineering, University at Buffalo, Buffalo, New York, USA

15 ⁶ Research and Education in eEnergy, Environment and Water (RENEW) Institute, University at Buffalo, Buffalo, New York, USA

⁷ Institute for Ion Physics and Applied Physics, University of Innsbruck, Innsbruck, Austria

⁸ Jet Propulsion Laboratory, California Institute of Technology, Pasadena, CA, USA

⁹ Environment and Climate Change Canada, Toronto ON, Canada

20 ¹⁰ Instrument Software and Science Data Systems, Pasadena, CA, USA

Correspondence: Karen Cady-Pereira (kcadyper@aer.com)

25 **Abstract.**

Ammonia is a significant precursor of PM_{2.5} particles and thus contributes to poor air quality in many regions. Furthermore, ammonia concentrations are rising due to the increase of large scale, intensive agricultural activities, which are often accompanied by greater use of fertilizers and concentrated animal feedlots. Ammonia is highly reactive, and thus highly variable and difficult to measure. Satellite based instruments, such as the Atmospheric Infrared Sounder (AIRS), and the Cross-Track Infrared Sounder (CrIS) sensors, have been shown to provide much greater temporal and spatial coverage of ammonia distribution and variability than is possible with in situ networks or aircraft campaigns, but the validation of these data is limited.

35 Here we evaluate ammonia retrievals from AIRS and CrIS against ammonia measurements from aircraft in the California Central Valley and in the Colorado Front Range. The satellite datasets were small and in California were obtained under difficult conditions. We show that the surface values of the retrieved profiles are biased very low in California and slightly high in Colorado, and that the bias appears to be primarily due to smoothing error. We also compare three years of CrIS ammonia against an in situ network in the Magic Valley in Idaho We show that CrIS ammonia



40 captures both the seasonal signal and the spatial variability in the Magic Valley, though it is biased low here also. In summary, analysis adds to the validation record but also points to the need for more validation under different conditions.

45 1. Introduction

Ammonia (NH_3) is one of the most common forms of reactive nitrogen and the primary alkaline gas in the atmosphere. Intended and unintended releases of NH_3 into the environment over the last century have significantly altered the natural nitrogen cycle (Erisman et al., 2008), so that the current emission levels of ammonia are about four times higher than in previous centuries
50 (Battye et al., 2017). The main sources of NH_3 are agricultural emissions, namely from livestock raising and fertilizer application (EDGAR-Emission Database for Global Atmospheric Research, 2014), which account for 80% of all emissions globally (Sutton et al., 2013; Behera et al., 2013). There are also some locally or seasonally significant sources NH_3 , the most notable being
55 biomass burning events, which can generate large amounts of NH_3 (Coheur et al., 2009; Whitburn et al., 2015, 2016). In urban areas automobiles with three-way catalytic converters (Sun et al., 2017) can be a major source of NH_3 . Nowak et al. (2012) estimate that in the Los Angeles basin cars contribute as much as 50% of the total NH_3 emissions.

Ammonia is the dominant base in the atmosphere, and it plays a significant role in the formation
60 of fine particulate matter ($\text{PM}_{2.5}$) (e.g., Aneja et al., 2003), which can penetrate deep into the lungs and severely impact the respiratory and circulatory systems (Pope et al., 2009). Paulot and Jacob (2014) have shown that the costs associated with the health impacts of NH_3 associated with food production for export in the US offset half the revenue from these exports. Long-term exposure to ambient $\text{PM}_{2.5}$ is the leading environmental risk factor for premature mortality
65 worldwide, leading to an estimated 2.5–3.4 million premature deaths annually (Cohen et al.,



2017), 20% of which is estimated to stem from NH₃ emissions (Lelieveld et al., 2015). Ammonia is not yet a criteria pollutant in the US (its emissions are regulated by the European Union (EU) and it is a criteria pollutant in Canada), but the EPA has published established regulations (<http://www.nslaw.com/single-post/2017/06/19/EPA-NSR-Chief-Outlines-NSR-Changes-at-2017-AWMA-Conference>) mandating that every state must set area specific significant emission rates (SERs) for NH₃. Since the emissions of NH₃ are a key factor in the formation of PM_{2.5}, reducing emissions can be an effective path to reduce air pollution (Liu et al., 2021). Given the rapid growth of industrial-scale agriculture (e.g., increase in egg, milk and meat consumption), especially in Asia (e.g., Xu et al., 2016), NH₃ emissions are projected to increase greatly over the next few decades in many parts of the world. The reduction of NO_x emissions due to more stringent controls will reduce the contribution of NO_x to the deposition of reactive nitrogen, but Paulot et al. (2013) suggest that an increase in NH₃ emissions will likely compensate for this reduction. NH₃ and its derivatives are also quickly deposited in the ecosystems, increasing their eutrophication and reducing biodiversity (Erisman et al., 2008). There is thus growing recognition that NH₃ is an important pollutant, and that it will likely play a greater role in air quality and ecosystem health over the next decades, due to both the essential role NH₃ plays in feeding the world's population, and to the fact that the atmospheric emission potential of NH₃ is directly linked to increasing temperatures (Skjøth et al., 2013; Sutton et al., 2013). However, in situ measurements remain a challenge. NH₃ is easy to detect, but it is hard to measure accurately. There are many in situ techniques used to detect atmospheric NH₃ with varying time resolution and precision, but the main issue affecting precision is the inlet rather than the instrument. NH₃ is sticky, and so it is challenging to get it into a given instrument quantitatively and quickly (Roscioli et al., 2016), (Pollack et al., 2019). This feature is critical for



characterizing the abundance of NH_3 in the background atmosphere, for making measurements
90 of NH_3 fluxes, and deploying instruments on aircraft. New open-path sensors avoid this issue,
but they cannot be deployed in many situations. Consequently, the emissions of NH_3 outside of a
limited set of well-instrumented locations remain poorly constrained, reducing the accuracy with
which models can represent concentrations and variability. The high spatial and temporal
variability of NH_3 exacerbates the lack of continuous, spatially well sampled data over extensive
95 regions. This also contributes to bottom-up inventories often underestimating emissions due to
scaling difficulties (Nowak et al., 2012).

Satellite data, even though they come with their own uncertainties, provide by virtue of their
spatial and temporal density, another option for quantifying these emissions. Currently there are
multiple NH_3 datasets, with varying data record lengths and spatial coverage, obtained from the
100 following instruments: the three Infrared Atmospheric Sounding Interferometer (IASI)
instruments flying in a 9:30 am orbit, the Greenhouse Gases Observing Satellite (GOSAT) in a
1:30 pm orbit, along with the Tropospheric Emission Spectrometer (TES), the Atmospheric
Infrared Sounder (AIRS), and the three Cross-Track Infrared Sounder (CrIS) instruments, all
flying in a 1:30 pm orbit. The data obtained from these instruments has had numerous
105 applications. Multiple papers (Van Damme et al., 2015; Shephard et al., 2011; Shephard and
Cady-Pereira, 2015; Warner et al.; 2016; Shephard et al., 2020, Wang et al., 2021) have shown
that NH_3 measurements from infrared sensors capture NH_3 hotspots, such as the Indo-Gangetic
plain, eastern China and the American Midwest, as well as the expected regional seasonal
variability and fire activity. Warner et al. (2017) used retrievals from AIRS to show definite
110 positive trends in NH_3 concentrations over the US, the EU and China, which the authors ascribe
to declines in SO_2 and NO_2 emissions in all three regions due to more stringent controls. Van



Damme et al. (2018) used nearly a decade of IASI data to show that the emissions listed in the EDGAR (EDGAR, 2016) inventory for large source regions were wrong by as much as a factor of three; furthermore, emissions from smaller sources were often underestimated by an order of magnitude. Dammers et al. (2019) found similar results using CrIS and IASI NH₃ data. Zhu et al. (2013) have demonstrated that Tropospheric Emission Spectrometer (TES) NH₃ data over North America in the 2006–2009 period, though relatively sparse, could be used in an inverse modeling framework to constrain emissions sufficiently to improve agreement between GEOS-Chem output and surface measurements from the National Atmospheric Deposition Program (NADP) Ammonia Monitoring Network (AMoN) network. Using NH₃ measurements from CrIS and NO₂ measurements from TROPOMI, Cao et al. (2022) demonstrated that NH₃ emissions decreased substantially over downtown Los Angeles during the 2019 March COVID-19 lockdown; this result is in agreement with the conclusion from Nowak et al. (2012) that in urban areas traffic can be a major source of NH₃ and consequently greatly increase exposure to PM_{2.5}.

Yet in spite of the increasing use of NH₃ data from space-based instruments, validation of these data remains rather limited. Sun et al. (2015) compared a small set of NH₃ total columns from the TES instrument against columns derived from surface and aircraft measurements during the NASA Deriving Information on Surface conditions from Column and Vertically Resolved Observations Relevant to Air Quality (DISCOVER-AQ) California 2013 campaign, and found small differences (less than 6%) and high correlation (R=0.82); however, note that TES, which is no longer operational, had much higher spectral resolution (0.06 cm⁻¹) and thus greater sensitivity to surface NH₃ and less interference from water vapor than the infrared sensors (AIRS, CrIS, IASI) currently providing data for NH₃ retrievals. Shephard et al. (2015) compared TES profiles against aircraft measurements taken during the 2013 Joint Canada–Alberta



135 Implementation Plan for Oil Sands Monitoring (JOSM) campaign and showed that the TES
profiles were unbiased. Warner et al. (2016) compared four NH₃ retrievals from AIRS against
aircraft profiles obtained during DISCOVER-AQ California and found good qualitative
agreement. Dammers et al. (2017) compared 218 IASI and CrIS total columns and CrIS profiles
140 against corresponding data from ground based Fourier Transform Infrared (FTIR) observations
at seven FTIR sites in the Network for the Detection of Atmospheric Composition Change
(NDACC): overall the FTIR and CrIS data were well correlated (R=0.77) and mainly unbiased.
Most of these FTIR stations in this analysis were located in high source regions, which
somewhat limits the applicability of these results to the regions of greatest interest to the air
quality community.

145 Van Damme et al. (2015) carried out what is likely the most extensive evaluation of NH₃
measured from space, comparing IASI NH₃ against data from six different monitoring networks
in North America, Europe, Africa and China and from the California Research at the Nexus of
Air Quality and Climate Change (CalNex) campaign in California. Most of the data from the
surface networks were provided on bi-weekly or monthly scales: when IASI columns were
150 converted to surface concentrations and averaged over the corresponding time period, they
showed qualitative agreement in space and time with the surface data: the correlations in general
were not high, though still significant. Recently Guo et al. (2021) (hereafter Guo2021) compared
NH₃ columns from IASI with integrated profiles obtained from aircraft data during the Colorado
2014 DISCOVER-AQ campaign: the IASI columns were unbiased and significantly correlated.

155 However, Guo2021 point out that the instruments currently used to measure NH₃ from aircraft
have large uncertainties due to limited accuracy and slow response to changing NH₃
concentrations.



To a varying degree all the studies above cite the same factors that complicate the validation of satellite NH₃ products:

- 160 • Sub-pixel inhomogeneity due to the high spatial-temporal variability of NH₃ driven by its short lifetime; thus the point data from an in situ instrument will only be partially correlated with the pixel scale data obtained from a satellite instrument
- Different measurement time scales (weeks or days vs instantaneous), especially for surface networks
- 165 • High instrument noise
- Validation results are strongly influenced by local atmospheric conditions and the vertical distribution of NH₃, which highlights the need for further validation campaigns under diverse conditions

Our objective is to add to the validation record at the single pixel scale with retrievals from L1B
170 radiances from both the AIRS and CrIS instruments. The retrieved profiles here are obtained with the MUlti-SpEctra, MUlti-SpECies, MUlti-Sensors (MUSES) (Fu et al., 2013, 2016, 2018) algorithm. which provides profiles, total columns and uncertainty estimates, all of which can also be evaluated against in situ data. AIRS and CrIS NH₃ will be compared against aircraft data from the P-3B aircraft flown during DISCOVER-AQ campaigns in California and Colorado. Warner
175 et al. (2016) also compared AIRS with DISCOVER-AQ, but their retrievals used cloud cleared radiances and covered nine AIRS pixels (~45 km footprints at nadir). Using single pixel radiances provides several advantages over “cloud cleared radiances”: the propagation of uncertainties from the radiances is simpler (see section 2.2) and the retrieved information is obtained on smaller scales, which is important for NH₃ (see section 5). This will be the first
180 comparison of single pixel NH₃ profiles from either AIRS or CrIS against aircraft data. While aircraft campaigns can provide snapshots in time, they do not provide sustained measurements



over strong point sources. In order to test the capability of MUSES NH₃ to capture temporal and spatial variability over an extended period, surface level CrIS NH₃ concentrations will also be evaluated against three years of data from a small monitoring network in the Magic Valley in Idaho. Section 2 will briefly review the NH₃ retrieval algorithm, section 3 will give an overview of the instruments, section 4 will present the analysis of the DISCOVER-AQ data and section 5 will follow with the analysis of the Magic Valley data; finally, section 6 will summarize our conclusions and discuss future work.

190 2. MUSES NH₃ Retrieval Algorithm

The first nadir retrievals of NH₃, obtained using a prototype retrieval with data from the TES instrument (Beer et al., 2008), exploited the NH₃ ν_2 vibrational band between 960 and 970 cm⁻¹ to demonstrate that TES could measure the variability in NH₃ along a transect in China. Shephard et al. (2011) implemented a full optimal estimation (OE) approach (Rodgers, 2000), which sought to reduce the difference between the measured CrIS radiances in ν_2 band and the calculated radiances from a radiative transfer model (Moncet et al., 2008). Before the OE algorithm was run an a priori profile was chosen from one of three possible profiles, representing background, moderate and enhanced NH₃ concentrations. These profiles were derived by binning global distributions of NH₃ (Shephard et al., 2011) from the chemical transport model GEOS-Chem (Zhu et al., 2013). The profile is selected by applying an online/offline brightness temperature (BT) difference test centered around the 967 cm⁻¹ line. The OE algorithm is then run as a refinement step, in which the a priori and the initial guess profiles are identical except for the background profile, for which the moderate profile is chosen as the initial guess, in order to provide Jacobians with some sensitivity.



205 The algorithm developed for the TES NH₃ retrievals has since been adapted with minor changes
for CrIS (Shephard and Cady-Pereira, 2015; Shephard et al., 2020) and AIRS (this paper). The
spectral retrieval window and the frequencies for the online/offline BT test were slightly
modified for the CrIS and AIRS spectral resolutions, and a preliminary retrieval step to adjust the
surface temperature and emissivity was introduced. This algorithm forms the core of the NH₃
210 component of the MUSES software used here and also of the CrIS Fast Physical Retrieval code,
whose product has been used in a number of previous studies (e.g., Shephard and Cady-Pereira,
2015; Shephard et al., 2020; Dammers et al. (2017); Cao et al. (2022), Marais et al. (2021)). The
two products have much in common (the same spectral microwindows, a priori selection,
constraint matrices and forward model), but obtain temperature and water profiles and surface
215 properties from different sources and use different software to carry out the optimal estimation.
Preliminary comparisons have shown excellent agreement between the two algorithms, but a full
comparison is beyond the scope of this paper, as the objective here is the validation of the
MUSES AIRS and CrIS NH₃ retrievals.

AIRS and CrIS NH₃ retrievals were both obtained by applying the MUSES algorithm to AIRS or
220 CrIS L1B single footprint radiances. The MUSES algorithm is an end-to-end optimal estimation
process that provides a complete characterization of the parameters involved in the radiative
transfer processes in the infrared region, using a multi-step approach. Before the NH₃ retrieval
step is reached, the atmosphere has been well characterized by the previous retrieval steps:
temperature and water vapor profiles, surface properties and cloud absorption are known and can
225 be accounted for in the NH₃ retrieval, significantly reducing errors from radiatively interfering
species. Since cloud optical depth is retrieved, cloud clearing algorithms (Susskind et al., 2003)
are not needed and retrievals can be performed on every pixel, or field of view (FOV), rather



than on the nine pixel field of regard (FOR). This allows for retrievals from AIRS with a 15 km rather than 45 km minimum footprint, which was the resolution for the earlier NH₃ retrievals from AIRS obtained by Warner et al. (2016) using cloud cleared radiances.

MUSES uses the Optimal Spectral Sampling (OSS) model (Moncet et al., 2008) as its forward model; OSS is a fast and accurate radiative transfer method designed specifically for the modeling of radiances measured by sounding radiometers in the infrared, although it is applicable throughout the microwave, visible, and ultraviolet regions.

Since the retrieval is non-linear, an a priori constraint is used for estimating the true state (Bowman et al., 2006). If the estimated (retrieved) state is close to the actual state, then the estimated state can be expressed in terms of the actual state through the linear retrieval (Rodgers, 2000):

$$\hat{\mathbf{x}} = \mathbf{x}_a + \mathbf{A}(\mathbf{x} - \mathbf{x}_a) + \mathbf{G}\mathbf{n} + \mathbf{G}\mathbf{K}_b(\mathbf{b} - \mathbf{b}_a) \quad (1)$$

where $\hat{\mathbf{x}}$, \mathbf{x}_a , and \mathbf{x} are the retrieved, a priori, and the “true” state vectors respectively, \mathbf{G} is the gain matrix, \mathbf{b} is the vector that contains parameters not retrieved in the current step and \mathbf{b}_a the a priori values for these parameters if they are retrieved in another step.

The averaging kernel, \mathbf{A} , describes the sensitivity of the retrieval to the true state:

$$\mathbf{A} = \frac{\partial \hat{\mathbf{x}}}{\partial \mathbf{x}} = (\mathbf{K}^T \mathbf{S}_n^{-1} \mathbf{K} + \mathbf{S}_a^{-1})^{-1} \mathbf{K}^T \mathbf{S}_n^{-1} \mathbf{K} = \mathbf{G}\mathbf{K} \quad (2)$$



where S_n is the instrument noise covariance matrix, and S_a is the a priori covariance matrix for the retrieval. The Jacobian, \mathbf{K} , is the sensitivity of the forward model radiances to the true state vector, $\mathbf{K} = \partial \mathbf{L} / \partial \mathbf{x}$. The rows of \mathbf{A} are functions with a finite width corresponding to the vertical resolution of the retrieved parameter. The sum of each row of \mathbf{A} provides a measure of retrieval information that comes from the measurement (Rodgers, 2000) at the corresponding altitude, provided that the retrieval is quasi-linear. The trace of the averaging kernel matrix gives the number of degrees of freedom for signal (DOFS) from the retrieval.

The total a posteriori error covariance matrix S_x for a given retrieved parameter $\hat{\mathbf{x}}$ is given by:

$$S_x = (\mathbf{A} - \mathbf{I})S_a(\mathbf{A} - \mathbf{I})^T + \mathbf{G}S_n\mathbf{G}^T + \mathbf{G}\mathbf{K}_bS_b(\mathbf{G}\mathbf{K}_b)^T \quad (3)$$

where S_b is the expected covariance of the non-retrieved parameters. The total error (or uncertainty) for a retrieved profile is expressed as the sum of: i) the smoothing errors (first term on the right-hand-side), i.e. the uncertainty due to unresolved fine structure in the profile; ii) the measurement errors (second term) originating from random noise in the spectrum; and iii) the systematic errors (last term) due to uncertainties in the forward model parameters not retrieved in the NH_3 step, some of which are constant and some of which change from retrieval-to-retrieval (Worden et al., 2006). For the current CrIS NH_3 algorithm this last term is not calculated and is not included in the total error estimate. By providing the expected error covariance and the averaging kernels, this approach facilitates the use of the retrieved profiles in inverse modeling efforts, since both terms are used to weight the information coming from the retrieval. The error covariance gives users an uncertainty estimate for each retrieved profile, which can be utilized to screen the data or be included in a statistical analysis. Furthermore, the estimated uncertainty



derived from the error covariance can be compared to measured uncertainties, obtained by
270 calculating the spread of the differences between satellite and in situ data, as will be shown in
sections 4.1 and 4.2; this analysis can indicate if there are error terms missing from the optimal
estimation formulation.

Rodgers and Connor (2003) presented a method for comparing satellite profiles of trace gases
with limited vertical resolution with in situ profiles obtained on a much finer grid. This approach
275 is often described as “applying the instrument operator” or “applying the averaging kernel”. It
attempts to estimate how the space based instrument would “see” an in situ profile by applying
the equation below to the in situ data:

$$\mathbf{X} = \mathbf{X}_{apriori} + \mathbf{A} (\mathbf{X}_{aircraft} - \mathbf{X}_{apriori}) \quad (4)$$

The estimated profile \mathbf{X} has been smoothed by the operator, simulating the smoothing due to the
280 coarser resolution of the satellite observation. When \mathbf{X} is compared to the satellite observations it
is assumed that the smoothing error has been accounted for and can be ignored, which is not the
case when satellite observations are compared directly to measured profiles; the remaining errors
will be due to instrument noise and temporal and spatial sampling differences; the latter can be
especially large for NH_3 , due to its large variability, as was discussed above. While we present
285 comparisons using the Rodgers and Connor approach, we will also show simple differences
between the aircraft and satellite data; there are many end-users who will want to use the data as
is in their own analysis and will want to know the corresponding uncertainties.

A note on applying the operator: AIRS and CrIS profiles extend to the top of the atmosphere,
while the aircraft profiles used here rarely go above 700 hPa in California and 500 hPa in
290 Colorado. We have therefore truncated the averaging kernels to these altitude ranges.

3. Data



3.1 Aircraft Data

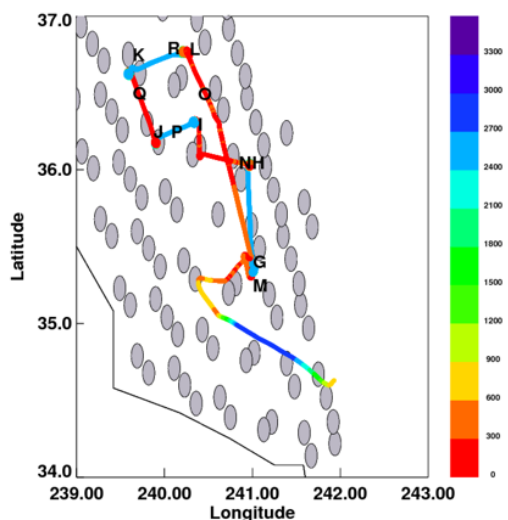


Figure 1: Sample aircraft track during DISCOVER-AQ in the Central Valley, CA; colors indicate altitude, letters locations of aircraft spirals; CrIS pixels are shown as grey ellipses

Vertical profiles of NH_3 were measured by the PTR-MS instrument (Muller et al. 2014) deployed aboard the NASA P3B aircraft during the NASA DISCOVER-AQ (Crawford and Pickering, 2014) campaigns in California in 2013 and Colorado in 2014. These campaigns were designed to validate collocated satellite observations of atmospheric pollutants over four regions in

the United States: (Maryland/Washington D.C, California, Texas and Colorado), but NH_3 was only measured in

California and Colorado. The P3B flight pattern was specifically designed for satellite validation: the aircraft flew repeated upward and downward spirals, typically 5 km wide connected by transects. An example trajectory, overlaid on the locations of CrIS NH_3 retrievals, is shown in Figure 1: the aircraft altitude is indicated by the colors, and the locations of the spirals are marked with letters. The PTR-MS instrument samples the atmosphere at 1Hz and the data were binned over 100 m to reduce noise. The estimated instrument uncertainty is 35% (Müller et al., 2014). Note that PTR-MS NH_3 data were a side product of the PTR-MS measurements during DISCOVER-AQ, which were designed to obtain data on volatile organic compounds (VOCs); this resulted in a higher detection limit and a slower response; the latter drawback leads to larger uncertainties when the NH_3 amounts are changing rapidly, as is the case when the aircraft is



leaving the boundary layer on upward spirals and entering the boundary layer on downward spirals.

3.2 Ground Data

320

The USDA-ARS Northwest Irrigation and Soils Research Laboratory established a regional NH₃ monitoring network in the Magic Valley region of south-central Idaho, USA utilizing the NADP AMoN network technology and protocols, but with much greater spatial density. The network measured ambient NH₃ concentrations along two transects of the Magic Valley (North-South and West-East) utilizing passive diffusive NH₃ samplers collected on a bi-weekly basis from February of 2018 through December of 2020. The objective of the project was to determine the spatial variability of ambient NH₃ concentrations across the region, which is dominated by agricultural production and high-density dairy operations, to better understand the potential for NH₃ transport within and downwind of the region.

330

3.3 Satellite data

3.3.1 AIRS single pixel NH₃ retrievals

AIRS is a nadir-viewing, scanning thermal infrared (TIR) spectrometer launched on board the Aqua satellite on May 4, 2002, into a sun synchronous polar orbit at an altitude of 705 km with a 1:30 am local solar time (LST) Equator in the ascending node and 1:30 pm (LST) in the descending node (Aumann et al., 2003). The daytime overpass is an ideal time for NH₃ retrievals, as thermal contrast is high and emissions are usually peaking, driven by higher temperatures. AIRS measures the thermal radiance between 3–12 microns with a spectral resolution of ~ 0.75 cm⁻¹ and a noise level of ~ 0.15K at 270 K (Zavyalov et al., 2013) in the 970 cm⁻¹ NH₃ absorption window. A single

340



AIRS FOV has a circular footprint with ~ 15 km diameter at nadir and the AIRS swath width is ~ 1650 , km which enables near global coverage twice daily.

3.3.2 CrIS single pixel NH_3 retrievals

CrIS is a Fourier Transform Infrared Radiometer (FTIR) launched on the Suomi National Polar
345 Orbiter Preparatory (SNPP) platform in October 2011 and on the Joint Polar Satellite System
(JPSS-1) in November 2017, into sun-synchronous orbits (824 km altitude) with the same LST
crossing times as AIRS; CrIS is a cross track scanning instrument with a 2200 km swath width
(± 50 degrees) with 14 km circular pixels (at nadir), a spectral resolution of 0.625 cm^{-1} and low
spectral noise ($\sim 0.04 \text{ K}$ at 270K) (Zavalyov et al., 2013) in the NH_3 spectral window. CrIS also
350 provides twice daily global coverage. Note that in this paper only CrIS data from the SNPP
platform have been used. There is a data gap in the SNPP-CrIS record between March and June
2019, corresponding to a malfunction in the electronics during that time.

4. DISCOVER-AQ Analysis

355 The DISCOVER-AQ campaigns in California and Colorado provide the most comprehensive set
of in situ NH_3 profile data (as opposed to retrievals from FTIR instruments) available. Though
limited to short (two month) periods in two strong source regions, these datasets can be used to
demonstrate the strengths and limitations of satellite data; additionally, they allow for the
evaluation of the accuracy of the retrieval estimated error, as calculated from Equation 3. During
360 each campaign the aircraft flew multiple up and down spirals. The satellite profiles were co-
located with aircraft profiles taken within one hour and 15 km of the satellite retrievals,
following the approach described in Guo2021. This co-location criterion is much stricter than is
usual for satellite validation (see Hegarty et al., 2022 for an example with CO retrievals from
AIRS) but is necessary given the variability in NH_3 (Guo2021). In consequence, each CrIS or



365 AIRS profile was compared with data from at most two spirals. Retrievals were checked for
quality by examining the root mean square (RMS) of the residuals and the retrieved cloud optical
depth. Comparing the aircraft and satellite profiles requires regridding the aircraft data to the
satellite vertical grid. This was accomplished by defining layers centered around each AIRS/CrIS
level, then finding the median value of the aircraft profile in each layer. The lowest layer
370 extended from the surface to the mid-point between the surface and the first AIRS/CrIS level
above the surface.

While both AIRS and CrIS have the same equatorial crossing time (~ 1:30pm local solar time),
this does not imply that both instruments are observing the same location at the same time at the
same angle. For example, on January 22, 2013, CrIS flew almost directly over the Central Valley
375 around 2100 UTC, while AIRS had its closest observation 15 degrees to the west around 2200
UTC, near the edge of its swath. Therefore, the set of aircraft profiles co-located with each
instrument is not identical.

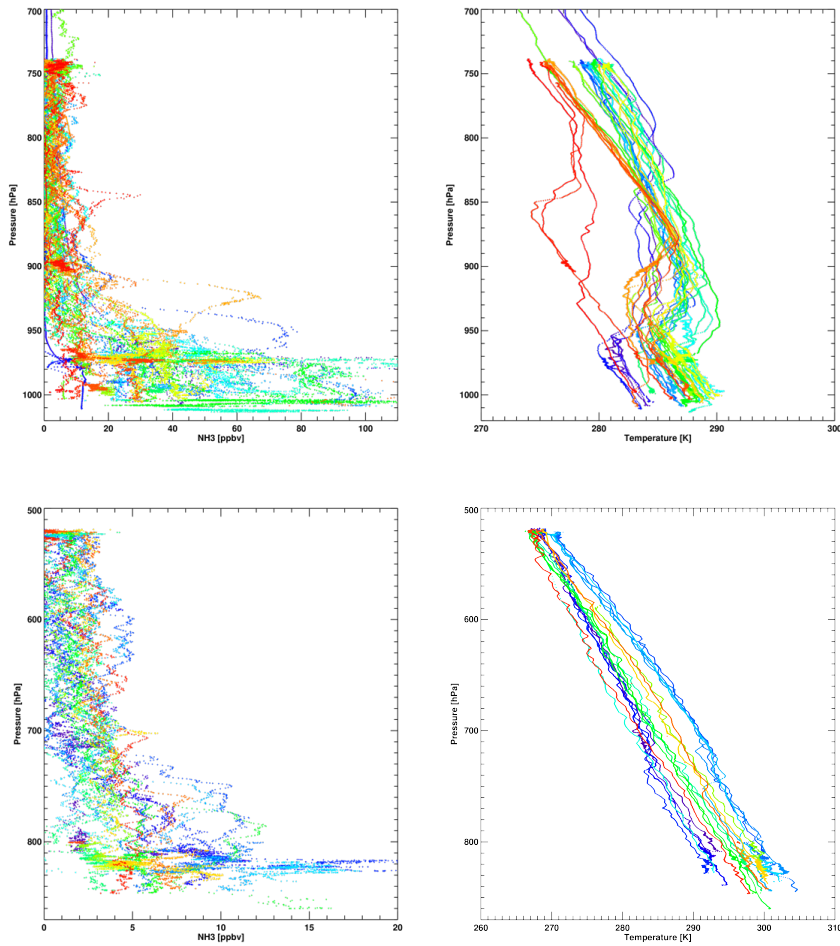
4.1 California

DISCOVER-AQ in California took place during January and February of 2013. The Central
380 Valley is one of the strongest NH₃ source regions in North America (e.g., Clarisse et al., 2009,
Shephard et al., 2020), and this was reflected in the aircraft data, which registered near surface
amounts as high as 100 ppbv (Figure 2, upper left panel). However, the observing conditions
were not ideal for satellite infrared retrievals, as there were thermal inversions over the entire
period (Figure 2, upper right). Inversions lead to increased uncertainties in the retrieval, as they
385 effectively create an emission layer above the surface, i.e., a layer that is warmer than the surface
and therefore emits more than it absorbs. Inversions also limit the vertical extent of the boundary
layer, with consequently lower NH₃ concentrations at altitudes where the retrieval has greater

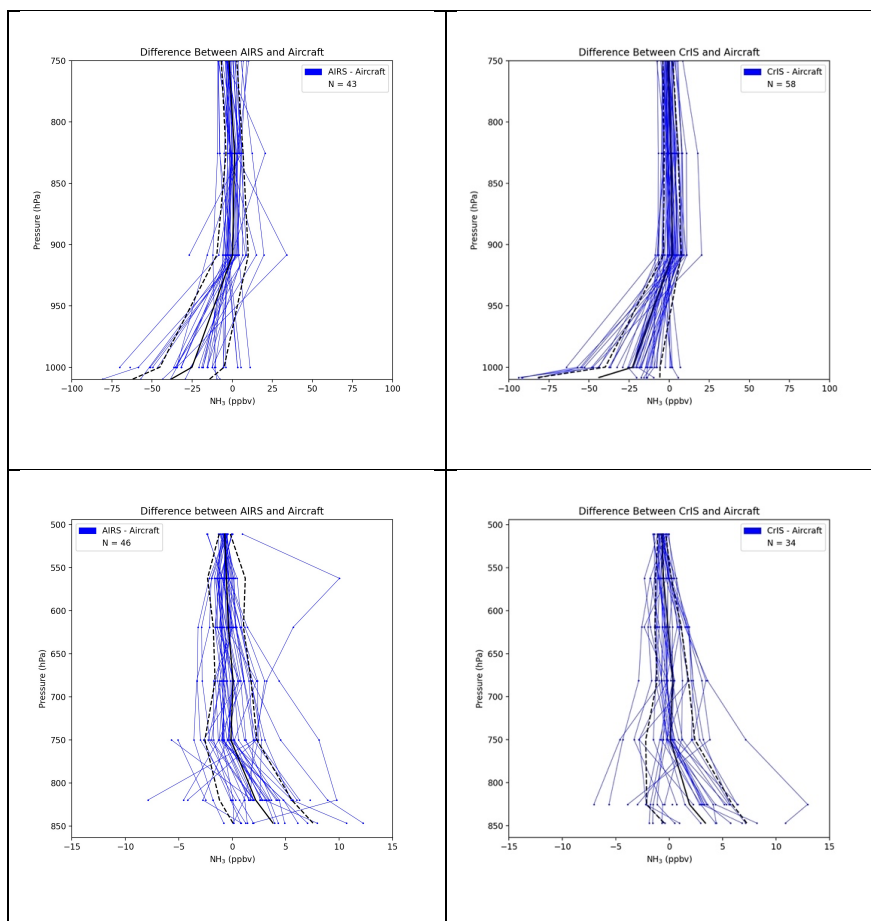


sensitivity. Nevertheless, evaluating the AIRS and CrIS NH₃ profiles against the aircraft data is still a useful exercise, as the combination of inversions and strong sources is not a unique
390 occurrence, and this analysis demonstrates the limitations of retrievals under these conditions. However, when averages over long periods and/or broad regions are desired, it would be reasonable to exclude cases with inversions.

43 AIRS and 58 CrIS profiles met the co-location criteria described above. When compared directly against the aircraft profiles (Figure 3, top panels), both instruments showed large
395 negative biases near the surface, as low as -80 ppbv for AIRS and -100 ppbv for CrIS, while the average bias at this level was ~-38 ppbv for AIRS and ~-44 ppbv for CrIS, with a spread of ~ 24 ppbv and 38 ppbv, respectively (Table I). This large negative bias is likely due to a combination of sub-pixel heterogeneity (Sun et al., 2015; Kille et al., 2019), the inherent difficulties of carrying out retrievals over thermal inversions, and smoothing errors. Clouds are accounted for
400 in the MUSES retrieval (Kulawik et al., 2006) and thus cloudy conditions should not significantly impact the NH₃ retrievals. Both the bias and the spread drop significantly with increasing altitude, as do the measured concentrations; while the biases decrease, they become positive and are not insignificant at 825 hPa (~30% at 825 hPa), and the spread is quite large (~100%) suggesting that at this altitude some of retrievals are overestimating the NH₃
405 concentrations with respect to the aircraft. The mean CrIS value at the surface (~16 ppbv) is 60% greater than the AIRS value (~10 ppbv); the lower CrIS noise level (0.04) vs AIRS (0.15) could allow for greater sensitivity to surface changes, in spite of the inversions.



410 *Figure 2: NH₃ profiles (left) obtained from aircraft during DISCOVER-AQ in California (top) and Colorado (bottom); only profiles co-located with CrIS data are shown; corresponding temperature profiles (right)*



415 *Figure 3: Difference between AIRS and aircraft NH₃ profiles (left) and CrIS and aircraft (right) during DISCOVER-AQ in California (top) and Colorado (bottom); solid line indicates mean bias and dashed lines standard deviations.*

The sum of the rows of the averaging kernels (SRAK) (Figure 4, top two panels), which provides an estimate of the retrieved information at each level originating from the measurement rather than from the a priori, shows for both AIRS and CrIS that while the information from the data peaks just below 700 hPa, the data also significantly contribute to the retrieved surface values.

420 The maximum SRAK (~1.2-1.3) is similar for both sensors, as is the SRAK at the surface (~0.6).

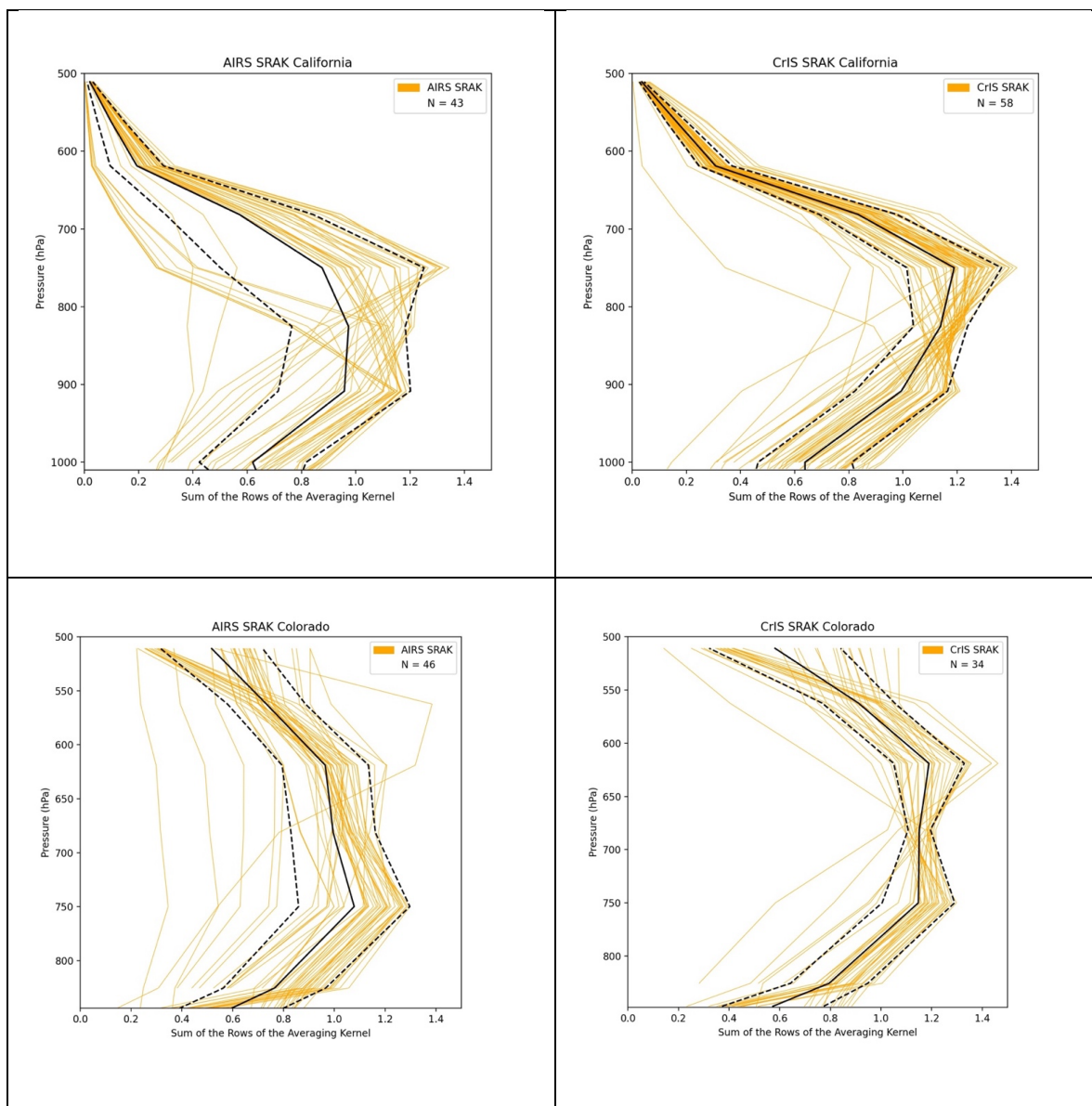
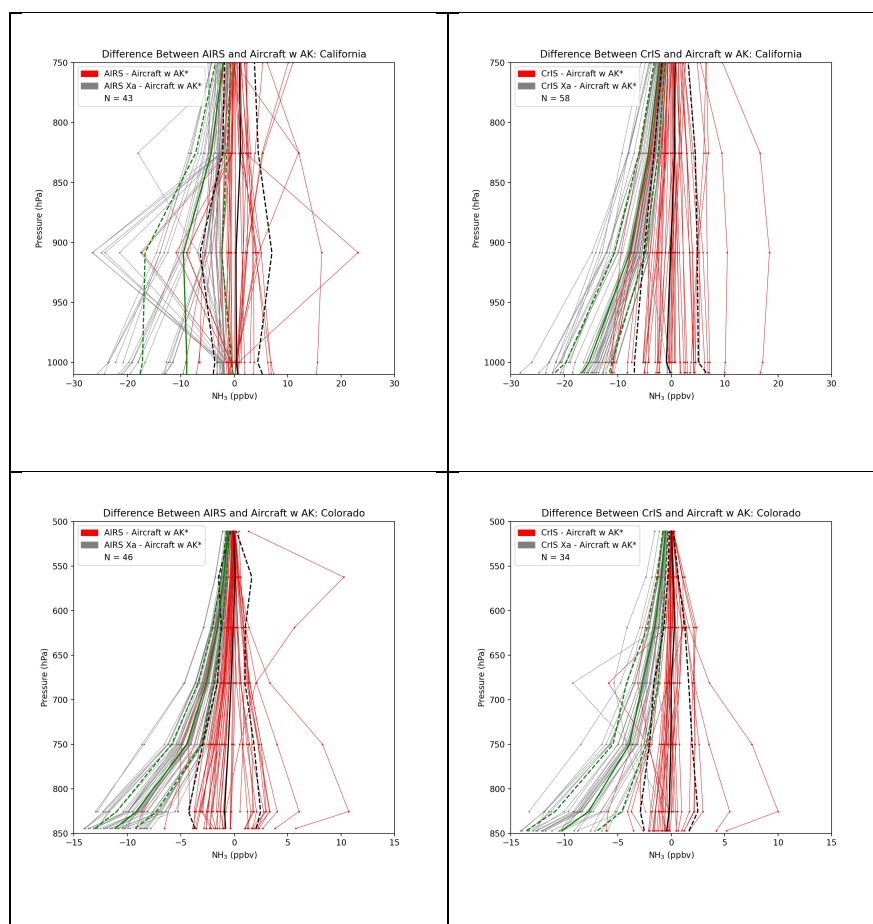


Figure 4: Sum of the row of the averaging kernels (SRAK) for AIRS (left panels) and CrIS (right panels); California (upper panels) and Colorado (lower panels)

However, there is much greater variability in the AIRS SRAK, possibly due to higher instrument
425 noise. Applying the instrument operators following equation 4 (Figure 5 (top panel), red and
black curves) reduces the bias at all levels to close to or less than 1.0 ppbv (Table 1, top section)



and dramatically reduces the spread at lower levels. These results indicate that the retrievals do not have significant systematic biases and that the bias in the direct comparisons originates from the a priori. If instead the a priori profiles are compared with the aircraft data, we see a large



430

435

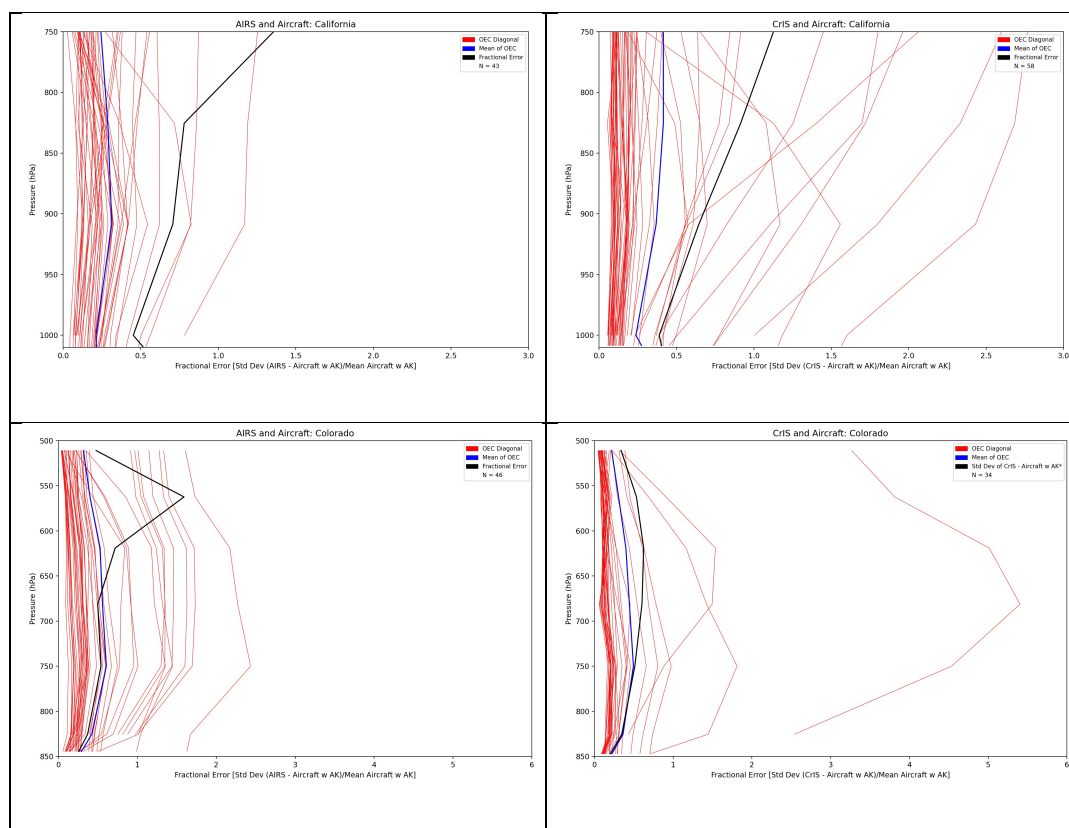
Figure 5: Difference between AIRS and aircraft NH_3 profiles (left) and CrIS and aircraft (right) during DISCOVER-AQ in California (top) and Colorado (bottom); the averaging kernel has been applied to the aircraft data; red lines show differences between the retrieved profiles and the aircraft data, black solid lines indicate mean bias and black dashed lines standard deviations; grey lines show differences between the a priori profiles and the aircraft, green solid lines indicate mean bias and green dashed lines standard deviations.

negative bias near the surface (~ 9 ppbv for AIRS and ~ 18 ppbv for CrIS). It has been argued that the a priori selection for these retrievals already uses all the information available in the



radiance data; this result demonstrates that the retrieval process does add significant information and reduces the a priori error.

440 The average estimated uncertainties from equation 3 (Figure 6, top panels, blue curves) are significantly lower than the measured uncertainties (the fractional standard deviation derived from the standard deviations of the differences in the “Satellite-Aircraft with AK” column in Table 1) (Figure 6, top panels, black curves) for both AIRS and CrIS, indicating that some error



445 *Figure 6: Fractional standard deviation between AIRS (left) and CrIS (right) and aircraft profiles with the averaging kernel applied (black) during DISCOVER-AQ in California (top panels) and Colorado (bottom panels); estimated uncertainty (red) and mean of estimated uncertainty (blue).*

sources are not accounted for in the optimal estimation process. The most likely source is the sampling difference: AIRS and CrIS sampled three dimensional columns, 15 to 50 km wide,

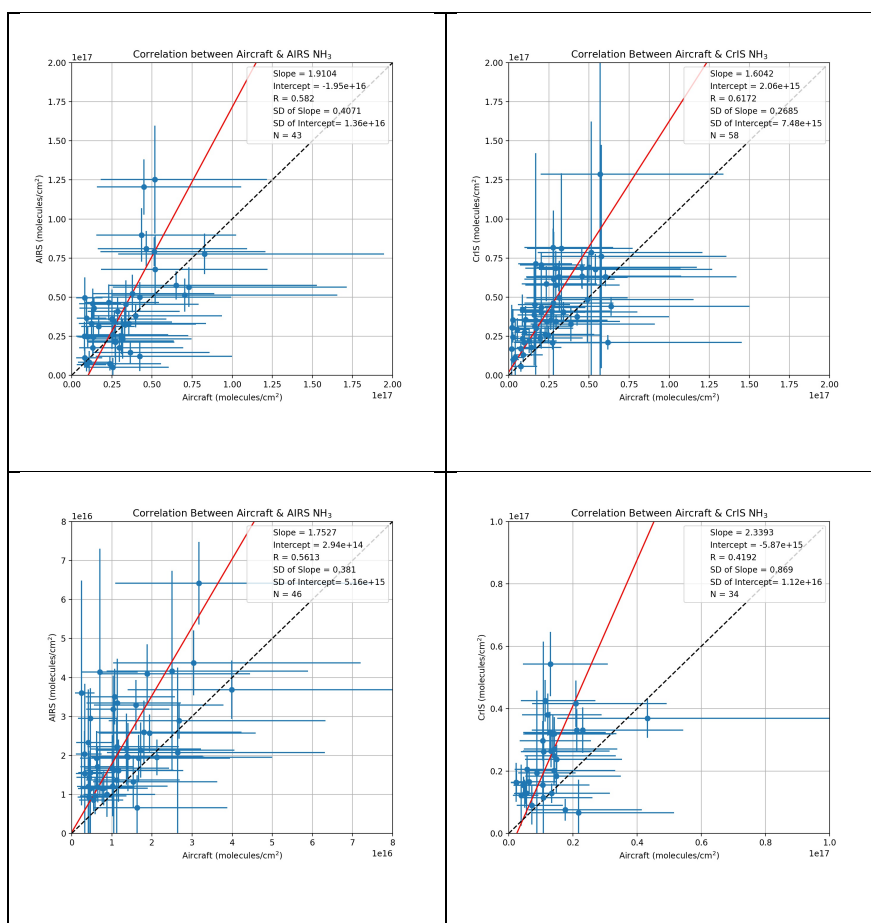


450 while aircraft instruments sampled in two dimensions, vertically and along a spiral line with a 5
 km width. Systematic retrieval errors, such as errors in water vapor, may also contribute. These
 fractional differences increase with altitude, but this is likely due to the rapid decrease in NH₃
 above the mixed layer, a case of large differences in small numbers. The measured uncertainties
 range from 5% to 50% in California. These large values point to the need for averaging over time
 455 or space to obtain less noisy information.

Table 1: Statistical analysis of the DISCOVER-AQ data from AIRS, CrIS and the aircraft over California in 2013 and Colorado in 2014.

California													
	Profile				Satellite-Aircraft: no AK				Satellite-Aircraft: with AK				
	Mean		Std Dev		Bias		Std Dev		Bias		Std Dev		
	AIRS	CrIS	AIRS	CrIS	AIRS	CrIS	AIRS	CrIS	AIRS	CrIS	AIRS	CrIS	
Pressure	hPa	ppbv	ppbv	ppbv	ppbv	ppbv	ppbv	ppbv	ppbv	ppbv	ppbv	ppbv	ppbv
1008.486	9.69	16.211	10.785	6.027	-38.03	-43.799	23.972	37.988	0.684	-0.171	4.593	6.716	
1000	9.342	14.443	9.875	5.44	-25.049	-22.746	19.995	17.106	0.396	-0.89	4.003	5.973	
908.514	9.693	7.63	8.634	4.101	0.238	1.956	9.81	5.582	0.344	-0.112	6.714	4.99	
825.402	5.742	4.883	5.401	3.372	1.471	1.266	5.327	4.345	1.186	0.653	3.328	3.854	
749.893	3.083	2.958	3.47	2.311	-1.96	-0.801	4.815	3.101	0.992	0.738	2.802	2.442	
Colorado													
	Profile				Satellite-Aircraft: no AK				Satellite-Aircraft: with AK				
	Mean		Std Dev		Bias		Std Dev		Bias		Std Dev		
	AIRS	CrIS	AIRS	CrIS	AIRS	CrIS	AIRS	CrIS	AIRS	CrIS	AIRS	CrIS	
Pressure	hPa	ppbv	ppbv	ppbv	ppbv	ppbv	ppbv	ppbv	ppbv	ppbv	ppbv	ppbv	ppbv
844.469	10.341	9.805	3.415	3.801	3.817	3.387	3.741	3.871	-0.803	-0.42	2.868	2.085	
825.402	8.214	7.529	3.064	3.595	2.19	1.902	3.377	4.006	-0.902	-0.193	3.368	2.687	
749.893	3.889	3.852	2.173	2.101	-0.12	0.102	2.431	2.292	-0.543	-0.031	2.392	1.994	
681.291	2.324	2.703	1.143	1.207	0.084	0.338	1.684	1.465	-0.288	0.012	1.3	1.626	
618.966	1.474	1.858	0.943	0.974	-0.356	-0.102	1.41	1.228	-0.083	0.304	1.119	0.972	
562.342	1.07	1.104	1.444	0.548	-0.538	-0.535	1.764	0.724	0.091	0.179	1.557	0.494	
510.898	0.521	0.552	0.231	0.212	-0.695	-0.687	0.523	0.374	-0.065	0.016	0.279	0.182	

Since much of the work on validating NH₃ from space-based infrared sensors has been done
 460 using IASI data, which provide total columns rather than profiles (e.g., van Damme et al., 2015;
 Dammers et al., 2017; Guo2021), here we also compare AIRS and CrIS total columns with
 aircraft total columns calculated using the mixed layer height approach described by Guo2021.



465 *Figure 7: total NH₃ columns from AIRS (left) and CrIS (right) versus aircraft columns during DISCOVER-AQ in California (top panels) and Colorado (bottom panels); dashed line shows the 1:1 line, red line the linear fit; vertical and horizontal lines indicate the uncertainties in the aircraft and satellite data, respectively.*

In this method the in situ NH₃ total column is estimated by integrating the aircraft NH₃ profile to the top of the mixed layer; above this level, NH₃ amounts are assumed to be zero. This is a
470 reasonable assumption, since NH₃ has a short lifetime (on the order of hours or days), and is rarely transported to the middle or upper troposphere; it has been measured above the mixed layer, but at low levels (less than 1 ppbv; e.g., Höpfner et al., 2019; Nowak et al., 2010). Furthermore, as stated in section 3.1, there are large uncertainties in the PTR-MS measurements above the mixed layer.



475 The MUSES total columns are compared against the integrated aircraft columns, using
orthogonal linear regression (Figure 7, top panels); the intercept has been allowed to vary, as
both AIRS and CrIS have detection limits, as does IASI. Note that the instrument operators have
not been applied to the aircraft column data. The correlation coefficients are 0.58 for AIRS and
0.62 for CrIS, within the range of results from previous studies. However, the slopes are very
480 much greater than one (1.9 for AIRS and 1.6 for CrIS), which was not the case in the IASI
evaluation of Guo2021. That study showed that assuming NH_3 concentrations are zero above the
mixed layer led to slopes close to the 1:1 line. If this assumption of zero amounts NH_3 above the
mixed layer is no longer valid at the later (13:30 LST) CrIS and AIRS overpass times, the
aircraft columns would be biased low with respect to CrIS and AIRS; on the other hand, the
485 profile differences shown in Figure 3 suggest that AIRS and CrIS are overestimating NH_3 above
910 hPa. Given the uncertainty in the aircraft measurements at these higher altitudes it is not
possible to currently resolve this issue.

4.2 Colorado

490 DISCOVER-AQ Colorado took place during July and August of 2014, in the Colorado Front
Range; while this is also a region with strong NH_3 sources, the aircraft data showed lower values
than in the California Central Valley (Figure 2, lower left panel); maximum values are on the
order of 20 ppbv, with most near surface values ranging from 5 to 10 ppbv. Also, in contrast to
the Central Valley there were no thermal inversions during this period (Figure 2, lower right
495 panel). Applying the co-location criteria yielded 46 AIRS profiles but only 34 CrIS profiles, in
part due to some poor quality CrIS retrievals. Direct comparisons of the AIRS and CrIS profiles
with aircraft data (Figure 3, lower panels) show both AIRS and CrIS biased high by 3.8 ppbv
(AIRS) and 3.4 ppbv (CrIS) near the surface (~ 844 hPa) and by 2.2 ppbv (AIRS) and 1.9 ppbv



(CrIS) at 825 hPa, but the bias is close to zero at 750 hPa. Note that this is in direct contrast to
500 the California results, which showed both AIRS and CrIS NH₃ biased very low at and near the
surface and biased slightly high at greater altitudes.

The sum of the rows of the averaging kernel plots (Figure 4, lower panels) present similar
maximum and surface values as in California, and applying the instrument operator again
eliminates the bias, but does not reduce the spread in the satellite-aircraft differences
505 dramatically (Figure 5, lower panels), while the large bias seen against the a priori profiles (~12
ppbv for AIRS and ~10 ppbv for CrIS) is removed by the retrieval, confirming again that the
retrieval process provides information content beyond the a priori.

The uncertainty analysis (Figure 6, lower panels) shows that the estimated uncertainty is quite
close to the measured uncertainty below 700 hPa, but is less than the measured value above this
510 level, indicating an unaccounted for error source. Finally, the total column comparisons also
indicate that the AIRS and CrIS NH₃ (Figure 7, lower panels) columns are correlated with the
aircraft values (with correlation coefficients of 0.56 for AIRS and 0.42 for CrIS), but are biased
high, most notably for CrIS, for which the regression presents a slope of 2.3. In this region the
high column biases are likely due to the bias in the retrieved surface and near surface values seen
515 in Figure 10, rather than differences between the retrieved and aircraft profile shape. Again, sub-
pixel heterogeneity and water vapor retrieval errors could also contribute to the differences.

5.0 Magic Valley Analysis

5.1 USDA network

520 The USDA-ARS established and maintained an NH₃ monitoring network along two transects
(North-South and West-East) across the Magic Valley region of south-central Idaho during the
February 2018-December 2020 period (Figure 8). The Magic Valley region is heavily dominated



525

530

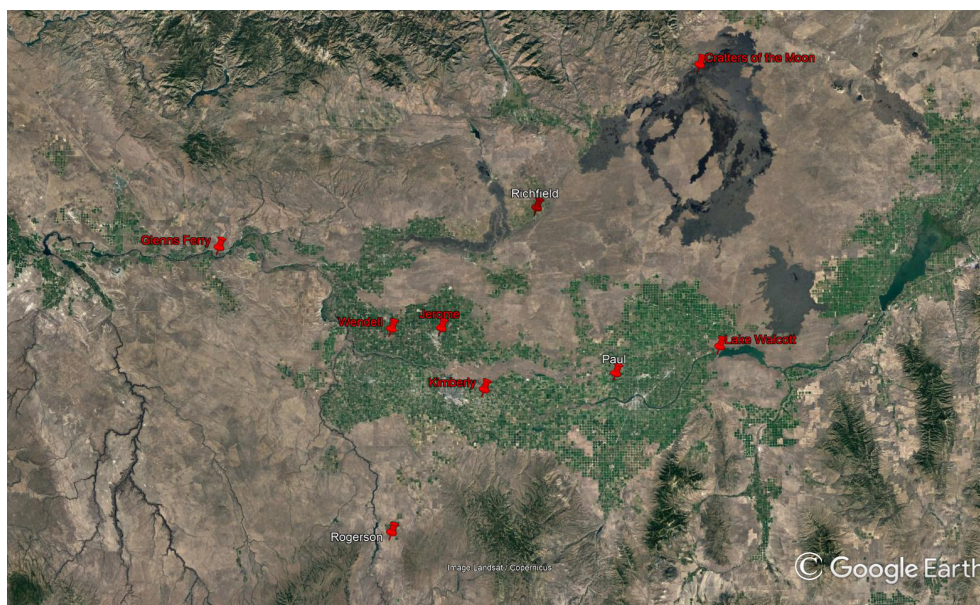


Figure 8: USDA Magic Valley network showing the nine measurement sites

535 by irrigated agriculture and is one of the most concentrated dairy production regions in the US
Research in this region has reported that NH_3 emissions from agricultural and dairy production
contribute approximately $44,000 \text{ MT N yr}^{-1}$ to the atmosphere (Leytem et al., 2021) and that NH_3
emissions fluctuate by season following trends in temperature (Leytem et al., 2011, 2013). The
network was established to gain a better understanding of the spatial variability of ambient NH_3
540 concentrations and transport within the region. The network consisted of 8 sampling locations (7
until 2020, when an additional site was added), and also utilized data from the NADP AMoN site
located to the north of the region at Craters of the Moon National Monument. Ammonia
concentrations were measured with passive diffusive NH_3 samplers (Radiello), which were
deployed bi-weekly, and generated two week mean surface NH_3 concentrations. Radiello
545 samplers have been shown to be approximately 9% biased high (Puchalski et al., 2015) These



data provided a unique opportunity to evaluate the seasonal signals measured by CrIS NH_3 , as well as its capability to capture small scale (on the order of a few kilometers) spatial variability.

5.2 Evaluating CrIS NH_3 against the surface data

CrIS NH_3 data are available for most of the 2018-2020 period, with a gap in the spring of 2019
550 due to an instrument malfunction. CrIS data within 15 km of each site were compared with the ground data at that site. Only the CrIS observations at CrIS ~13:30 LST were analyzed. The NH_3 retrievals at 1:30 LST have weaker signals (due to lower thermal contrast), and would add uncertainty to the results; furthermore, while there are strong diurnal cycles in the NH_3 emitted from the dairy facilities (Letyem et al., 2011, 2013) the average daily emissions are close to the
555 early afternoon value. Figure 9 shows the individual CrIS observations (small red triangles), the two-week averages of the CrIS data (large red triangles connected with a red line) and the ground data (blue triangles) at each site.

The time series in Figure 9 are sorted by the peak values of the ground data. At every site, CrIS clearly captures the seasonal cycle, though winter values are usually underestimated (possibly,
560 and a few strong warm season peaks in the ground data are not observed. At Craters of the Moon, a National Monument, and at Rogerson, in land administered by the Bureau of Land Management, CrIS returns consistently higher values than the ground site during the warmer months (May to October). At present we have no explanation for this high bias. At the next four site (Glenns Ferry, Richfield, Lake Wolcott and Kimberley), which are in areas of mixed
565 agricultural activity, CrIS and the ground data are in good agreement during the warmer months, though CrIS underestimates the June 2018 maximum at the Richfield site. At all four sites there is a peak in the ground data in November 2019 that is either matched in the CrIS data (Glenns Ferry) or at least visible (Richfield, Kimberley, Lake Wolcott). This peak is also evident in the



570 data from Paul and possibly Wendell, though the variability at this latter site makes it difficult to confirm. This suggests an area wide change in meteorological conditions, such as an inversion,

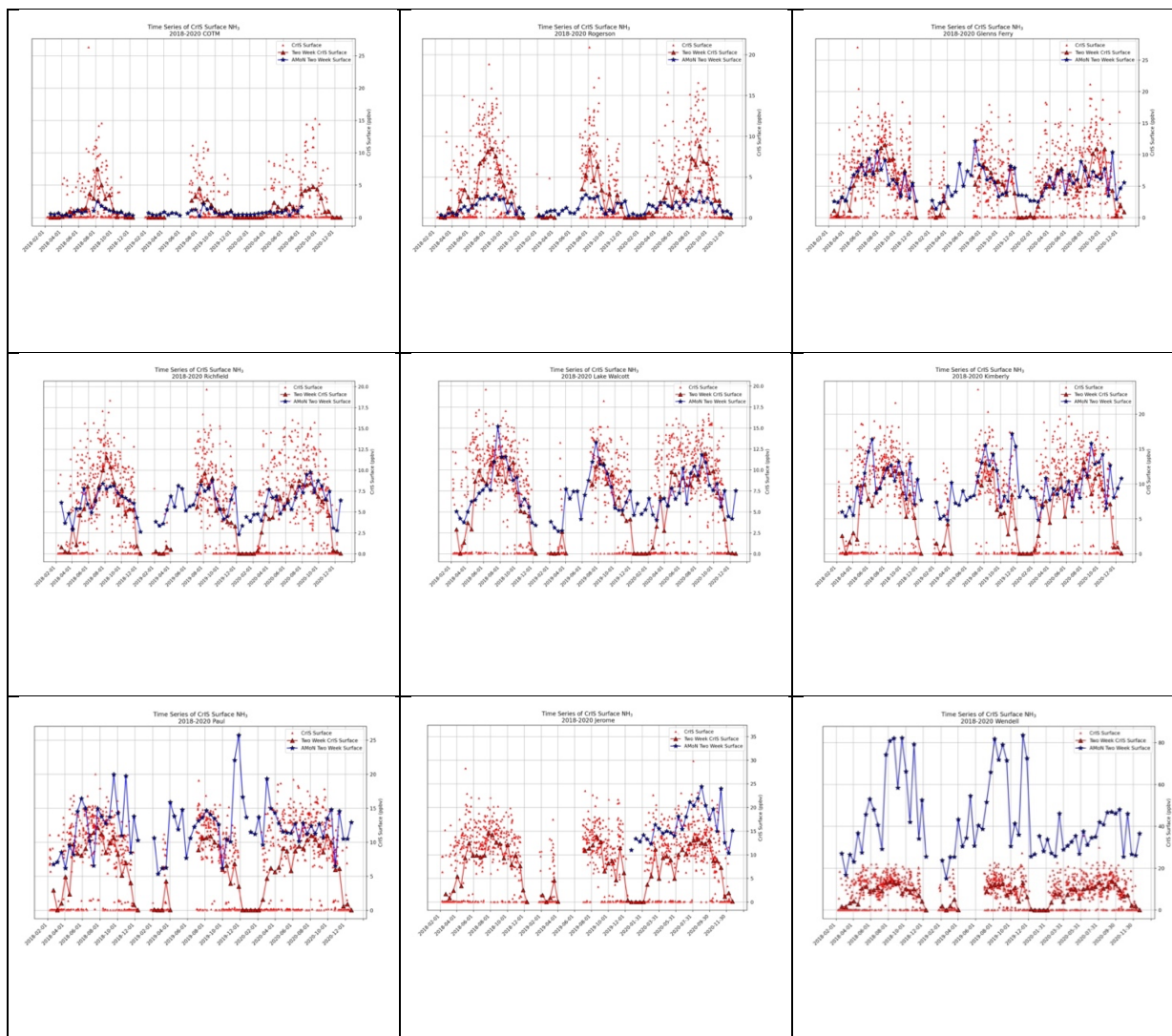


Figure 9: Time series of the in situ data (blue triangles, and the collocated CrIS surface values; red dots indicate daily values, red triangles two week means.

575 that led to increased NH_3 near the surface: however, there is no evidence in the meteorological data for such an inversion. The last three sites (Paul, Jerome and Wendell) are close to and/or downwind of multiple dairies, which likely leads to greater sub-pixel inhomogeneity. CrIS



underestimates the warm season maximum, and does not capture many of the peaks in the ground data, most notably at the Wendell site, where CrIS did not observe the over 80 ppbv peaks in 2018 and 2019; these extremely high concentrations were not observed in 2020. The sudden change suggests that a strong source that was dominating the signal in the ground data stopped emitting in 2020.

Analyzing these data in aggregate, first spatially then temporally, provides some useful insights.

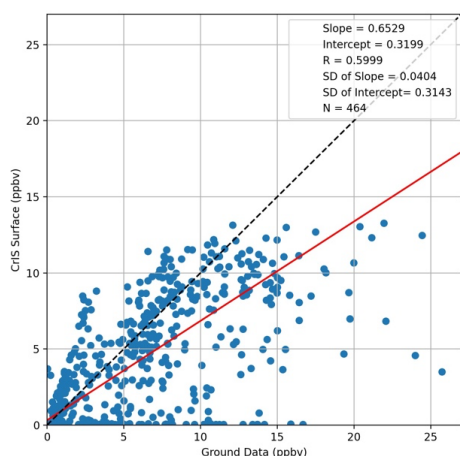


Figure 10: two week means of surface NH₃ from CrIS and the in situ instruments; dashed line shows the 1:1 line, red line the linear fit.

Plotting the CrIS two week averages against all the ground data values (Figure 10), excluding those from the Wendell site, which are extreme outliers, shows a correlation of 0.6, at the high end of the values reported in the literature and slope of 0.65, indicating that CrIS NH₃ is biased low overall. This result is in line with the low biases found in the surface values of the AIRS and CrIS California data, though here not necessarily caused by thermal

inversions, and with the low biases in the CFPR results at high NH₃ FTIR values seen by Dammers et al. (2017). It provides a quantitative measure of the agreement seen in the seasonal cycles shown in Figure 9.

Three years of fairly dense data over a region with many sources with fixed locations are an excellent candidate for spatial oversampling algorithms, which trade temporal resolution for greater information on spatial variability. Here we applied the physics based oversampling algorithm developed by Sun et al. (2018), which uses the instrument spatial response function to



600 weight the contributions of each satellite observation to a fine grid (here 0.002 deg), to each of
the three years of CrIS data taken over the Magic Valley region (Figure 11). The in-situ data are
overlaid on the CrIS maps; note that the Wendell values are shown in the upper right corner of
the maps, as otherwise they would distort the color scale; note also that the Jerome data are blank
in 2018 and 2019, when this site was not operational.

605

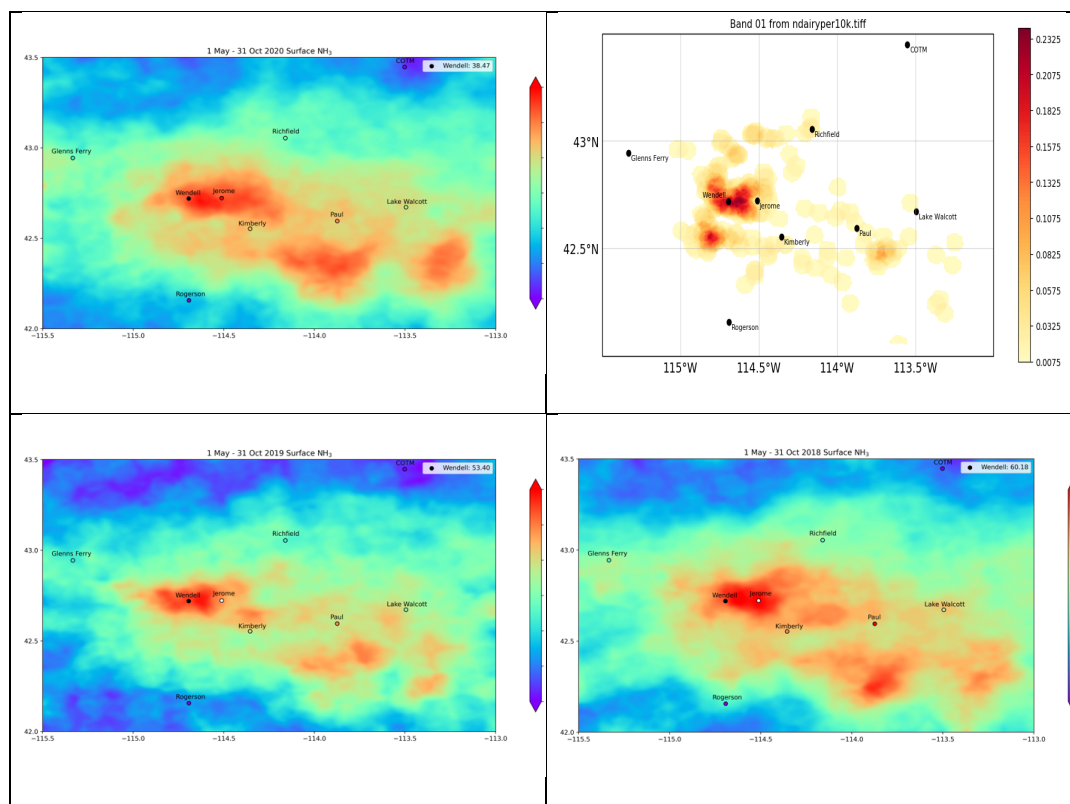


Figure 11: CrIS surface NH₃ data from the May to October period oversampled onto a 0.002 deg grid for each of three years: 2020 (upper left), 2019 (lower left), 2018 (lower right); number of dairies per square kilometer (upper right)

The location of the CrIS NH₃ “hotspots” and the gradients in NH₃ are very consistent from year
610 to year, though NH₃ concentrations are lower in 2019, possibly due to the CrIS data gap between
March and June. There is good qualitative agreement with the in situ data, with the exception of



the Wendell site, which was discussed above. Moreover, the hotspots are very well correlated with the areas of high dairy density (Figure 11, upper right). These maps illustrate the power of the CrIS data to provide context to in situ measurements and far more information on the spatial variability in NH_3 than is normally available from emissions databases, which are frequently at county level. Data from these gridded maps could be used to constrain emission inventories over much larger areas and at more frequent intervals than is currently possible. This oversampling analysis demonstrates the utility of providing users with Level 2 products, since they then choose the sampling periods and resolution that are most appropriate for their purposes and are best suited to the times and regions under investigation. For example, a user might want to study the variability of NH_3 over just the urban area of Mexico City. Level 3 products provide no such flexibility.

6.0 Conclusions and future work

While the DISCOVER-AQ datasets are limited in their temporal and spatial coverage, and in challenging conditions in California, they do provide some useful information for end-users who would like to use CrIS and AIRS data over strong source regions. The AIRS and CrIS profiles individually have large uncertainties, which are driven by local conditions, most significantly temperature profiles and sub-pixel heterogeneity. However, average biases, after smoothing errors are accounted for, are below or close to 1 ppbv. The error analysis in Figures 7 and 13 indicates that the a posteriori estimated error underestimates the actual uncertainties: this is likely caused by differences in the air masses sampled by the satellite and the aircraft measurements., and to a lesser extent by unaccounted for error sources. The column data suggest that either there is more NH_3 than expected above the mixed layer, or the retrievals are overestimating NH_3 above



this layer, maybe because the a priori profile shape is very different from the true profile shape.

635 More measurements of NH_3 in this altitude region are required to resolve this issue.

The Magic Valley analysis clearly demonstrates the importance of having more than a few dozen data point measurements to obtain useful information from space-based retrievals of NH_3 . With 464 observations over three years, over a limited region, it was possible to obtain a clear picture of the source distribution in the Magic Valley through the application of a physics based

640 oversampling algorithm. Further work will apply this approach to other regions and times and use the resulting maps to estimate emissions and to improve reactive nitrogen deposition estimates.

Acknowledgements:

645

Part of this research was carried out at the Jet Propulsion Laboratory (JPL), California Institute of Technology, under a contract with NASA. Susan Kulawik made substantial contributions to the development of the MUSES algorithms and software at JPL.

650 This research has been supported by NASA via the Tropospheric Ozone and its Precursors from Earth System Sounding (TROPOSS) project at JPL and by a Suomi National Polar-Orbiting Partnership (NPP) and the Joint Polar Satellite System (JPSS) Satellites Standard Products for Earth System Data Records grant (80NSSC21K1963) to Karen Cady-Pereira at AER.

655 This research was also supported, in part, by the U.S. Department of Agriculture, Agricultural Research Service. Mention of trade names or commercial products in this publication is solely for the purpose of providing specific information and does not imply recommendation or endorsement by the U.S. Department of Agriculture. USDA is an equal opportunity provider and employer.

660

NH_3 measurements during DISCOVER-AQ were supported by the Austrian Federal Ministry for Transport, Innovation and Technology (bmvit) through the Austrian Space Applications Programme (ASAP) of the Austrian Research Promotion Agency (FFG) (grants #833451, #840086). Tomas Mikoviny is acknowledged for field support; Ionicon Analytik is

665 acknowledged for instrumental support.

Kang Sun acknowledges support from NASA ACPMAP (80NSSC19K0988).



670

Data availability

MUSES AIRS and CrIS NH₃ products from S-NPP are available via the GES-DISC from the NASA Tropospheric Ozone and Precursors from Earth System Sounding (TROPESS) project at https://disc.gsfc.nasa.gov/datasets/TRPSDL2NH3AIRSFS_1/summary?keywords=tropess%20nh3. (Bowman, 2021a) and https://disc.gsfc.nasa.gov/datasets/TRPSDL2NH3CRSFS_1/summary?keywords=tropess%20nh3. (Bowman 2021b) respectively. The AIRS and CrIS datasets matched with aircraft used here for validation are available from the authors on request.

680 Author contributions

KCP designed the project, carried out the MUSES retrievals, created the preliminary plots, analyzed the results and wrote the manuscript. XG, RW and MZ provided the co-located aircraft data and made suggestions for the manuscript. AL provided the Magic Valley data and contributed relevant text. KS provided the oversampling code and revised the manuscript. VP and MS provided useful insights and revised the manuscript. CC and EB created all the plots. MM and AW obtained the DISCOVER-AQ data. VK designed and built the MUSES software.

References

690

- Aneja, V. P., Nelson, D. R., Roelle, P. A., Walker, J. T., and Battye, W.: Agricultural ammonia emissions and ammonium concentrations associated with aerosols and precipitation in the southeast United States, *J. Geophys. Res.*, 108(D4), 4152, <https://doi.org/10.1029/2002JD002271>, 2003.
- 695 Aumann, H. H., Chahine, M. T., Goldberg, M. D., Kalnay, E., McMillin, L. M., Revercomb, H., Rosenkranz, P. W., Smith, W. L., Staelin, D. H., Strow, L. L., and Suskind, J.: AIRS/AMSU/HSB on the Aqua mission: Design, science objectives, data products and processing systems, *IEEE T. Geosci. Remote*, 41, 253–264, 2003.
- Battye, W., Aneja, V. P., and Schlesinger, W. H.: Is nitrogen the next carbon? *Earth's Future*, 5(9), 894–904, 2017.
- 700 Beer, R., Shephard, M. W., Kulawik, S. S., Clough, S. A., Eldering, A., Bowman, K. W., Sander, S. P., Fisher, B. M., Payne, V. H., Luo, M., Osterman, G. B., and Worden, J. R.: First satellite observations of lower tropospheric ammonia and methanol, *Geophys. Res. Lett.*, 35, L09801, <https://doi.org/10.1029/2008GL033642>, 2008.



- 705 Behera, S. N., Sharma, M., Aneja, V. P., and Balasubramanian, R.: Ammonia in the atmosphere: A review on emission sources, atmospheric chemistry and deposition on terrestrial bodies, *Environ. Sci. Pollut. R.*, 20(11), 8092–8131, <https://doi.org/10.1007/s11356-013-2051-9>, 2013.
- Bowman, K. W., Rodgers, C. D., Kulawik, S. S., Worden, J., Sarkissian, E., Osterman, G., Steck, T., Lou, M., Eldering, A., and Shephard, M.: Tropospheric emission spectrometer: Retrieval method and error analysis, *IEEE T. Geosci. Remote*, 44(5), 1297–1307, 2006.
- 710 Bowman, K. W., TROPES AIRS-Aqua L2 Ammonia for Forward Stream, Standard Product V1, Greenbelt, MD, USA, Goddard Earth Sciences Data and Information Services Center (GES DISC), [10.5067/EYXLPVGTSWFF](https://doi.org/10.5067/EYXLPVGTSWFF), 2021a.
- 715 Bowman, K. W., (TROPES CrIS-SNPP L2 Ammonia for Forward Stream, Standard Product V1, Greenbelt, MD, USA, Goddard Earth Sciences Data and Information Services Center (GES DISC), [10.5067/B4TF7ND8A3O7](https://doi.org/10.5067/B4TF7ND8A3O7), 2021b.
- Cao, H., Henze, D. K., Cady-Pereira, K., McDonald, B. C., Harkins, C., Sun, K., Bowman, K. W., Fu, T.-M. and Nawaz, M. O.: COVID-19 lockdowns afford the first satellite-based confirmation that vehicles are an under-recognized source of urban NH₃ pollution in Los Angeles, *Environ. Sci. Tech. Let.*, 9(1), 3–9, <https://doi.org/10.1021/acs.estlett.1c00730>, 2022.
- 720 Cohen, A. J., Aaron, J., Brauer, M., Burnett, R., Anderson, H. R., Frostad, J., Estep, K., Balakrishnan, K., Brunekreef, B., Dandona, L., Dandona, R., Feigin, V., Freedman, G., Hubbell, B., Jobling, A., Kan, H., Knibbs, L., Liu, Y., Martin, R., Morawska, L., Pope, C. A., Shin, H., Straif, K., Shaddick, G., Thomas, M., van Dingenen, R., van Donkelaar, A., Vos, T., Murray, C., Forouzanfar, J. L., Mohammad, H.: Estimates and 25-year trends of the global burden of disease attributable to ambient air pollution: an analysis of data from the Global Burden of Diseases Study 2015, *The Lancet*, 389 (10082), 1907–1918, 2017.
- 725 Coheur, P. F., Clarisse, L., Turquety, S., Hurtmans, D., and Clerbaux, C.: IASI measurements of reactive trace species in biomass burning plumes, *Atmos. Chem. Phys.*, 9(15), 5655–5667, <https://doi.org/10.5194/acp-9-5655-2009>, 2009.
- 730 Crawford, J. H., and Pickering, K. E.: DISCOVER-AQ: Advancing strategies for air quality observations in the next decade, *EM Magazine*, Air & Waste Management Association, 9, 4–7. Retrieved from <https://www.awma.org/content.asp?admin=Y&contentid=301>, 2014.
- 735 Dammers, E., Shephard, M. W., Palm, M., Cady-Pereira, K., Capps, S., Lutsch, E., Strong, K., Hannigan, J. W., Ortega, I., Toon, G. C., Stremme, W., Grutter, M., Jones, N., Smale, D., Siemons, J., Hrpcek, K., Tremblay, D., Schaap, M., Notholt, J., and Erisman, J. W.: Validation of the CrIS fast physical NH₃ retrieval with ground-based FTIR, *Atmos. Meas. Tech.*, 10, 2645–2667, <https://doi.org/10.5194/amt-10-2645-2017>, 2017.
- 740 Dammers, E., McLinden, C. A., Griffin, D., Shephard, M. W., Van Der Graaf, S., Lutsch, E., Schaap, M., Gainairu-Matz, Y., Fioletov, V., Van Damme, M., Whitburn, S., Clarisse, L., Cady-Pereira, K., Clerbaux, C., Coheur, P. F., and Erisman, J. W.: NH₃ emissions from large point sources derived from CrIS and IASI satellite observations, *Atmos. Chem. Phys.*, 19, 12261–12293, <https://doi.org/10.5194/acp-19-12261-2019>, 2019.
- 745 Emission Database for Global Atmospheric Research (EDGAR), release version 4.3.1, <http://edgar.jrc.ec.europa.eu/overview.php?v=431> (2016).



- 750 Erisman, J. W., Sutton, M. A., Galloway, J., Klimont, Z., and Winiwarer, W.: How a century of ammonia synthesis changed the world? *Nat. Geosci.*, 1(10), 636–639, <https://doi.org/10.1038/ngeo325>, 2008.
- Fu, D., Worden, J. R., Liu, X., Kulawik, S. S., Bowman, K. W., and Natraj, V.: Characterization of ozone profiles derived from Aura TES and OMI radiances, *Atmos. Chem. Phys.*, 13(6), 3445–3462, <https://doi.org/10.5194/acp-13-3445-2013>, 2013.
- 755 Fu, D., Bowman, K. W., Worden, H. M., Natraj, V., Worden, J. R., Yu, S., Veefkind, P., Aben, I., Landgraf, J., Strow, L., and Han, Y.: High-resolution tropospheric carbon monoxide profiles retrieved from CrIS and TROPOMI, *Atmos. Meas. Tech.*, 9, 2567–2579, <https://doi.org/10.5194/amt-9-2567-2016>, 2016.
- 760 Fu, D., Kulawik, S. S., Miyazaki, K., Bowman, K. W., Worden, J. R., Eldering, A., Livesey, N. J., Teixeira, J., Irion, F. W., Herman, R. L., Osterman, G. B., Liu, X., Levelt, P. F., Thompson, A. M., and Luo, M.: Retrievals of tropospheric ozone profiles from the synergism of AIRS and OMI: methodology and validation, *Atmos. Meas. Tech.*, 11(10), 5587–5605, <https://doi.org/10.5194/amt-11-5587-2018-supplement>, 2018.
- 765 Guo, X., Wang, R., Pan, D., Zondlo, M.A., Clarisse, L., Van Damme, M., Whitburn, S., Coheur, P.-F., Clerbaux, C., Franco, B., Golston, L. M., Wendt, L., Sun, K., Tao, L., Miller, D., Mikoviny, T., Muller, M., Wisthaler, A., Tevlin, A. G., Murphy, J. G., Nowak, J. B., Roscioli, J. R., Vokamer, R., Kille, N., Neuman, J. A., Eilerman, S. J., Crawford, J. H., Yacovitch, T. A., Barrick, J. D., Scarino, A. J.: Validation of IASI satellite ammonia observations at the pixel scale using in situ vertical profiles, *J. Geophys. Res.-Atmos.*, 126, e2020JD033475, <https://doi.org/10.1029/2020JD033475>, 2021.
- 770 Hegarty, J. D., Cady-Pereira, K. E., Payne, V. H., Kulawik, S. S., Worden, J. R., Kantchev, V., Worden, H. M., McKain, K., Pittman, J. V., Commane, R., Daube Jr., B. C., and Kort, E. A.: Validation and error estimation of AIRS MUSES CO profiles with HIPPO, ATom, and NOAA GML aircraft observations, *Atmos. Meas. Tech.*, 15, 205–223, <https://doi.org/10.5194/amt-15-205-2022>, 2022.
- 775 Höpfner, M., Ungermann, J., Borrmann, S., Wagner, R., Spang, R., Riese, M., Stiller, G., Appel, O., Batenburg, A., Bucci, S., Cairo, F., Dragoneas, A., Friedl-Vallon, F., Hünig, A., Johansson, S., Krasaukas, L., Legras, B., Leisner, T., Mahnke, C., Möhler, O., Molleker, S., Müller, R., Neubert, T., Orphal, J., Preusse, P., Rex, M., Saathoff, H., Stroh, F., Weigel, R., and Wohltmann, I.: Ammonium nitrate particles formed in upper troposphere from ground ammonia sources during Asian monsoons, *Nat. Geosci.*, 12(8), 608–612, <https://doi.org/10.1038/s41561-019-0385-8>, 2019.
- 780 Kille, N., Chiu, R., Frey, M., Hase, F., Sha, M. K., Blumenstock, T., et al. (2019). Separation of methane emissions from agricultural and natural gas sources in the Colorado Front Range. *Geophysical Research Letters*, 46(7), 3990–3998. <https://doi.org/10.1029/2019GL082132>
- 785 Kulawik, S. S., Worden, J., Eldering, A., et al., Implementation of cloud retrievals for Tropospheric Emission Spectrometer (TES) atmospheric retrievals: 1. Description and characterization of errors on trace gas retrievals, *J. Geophys. Res.*, 111, D24204, doi:10.1029/2005JD006733, 2006.
- 790 Lelieveld, J.; Evans, J. S.; Fnais, M.; Giannadaki, D.; Pozzer, A. The contribution of outdoor air pollution sources to premature mortality on a global scale. *Nature*, 525, 367–371, 2015.



- Leytem, A. B., Dungan, R. S., Bjerneberg, D. L., and Koehn, A. C.: Emissions of ammonia, methane, carbon dioxide, and nitrous oxide from dairy cattle housing and manure management systems, *J. Environ. Qual.*, 40:1383–1394, 2011.
- 795 Leytem, A. B., Dungan, R. S., Bjerneberg, D. L., and Koehn, A. C.: Greenhouse gas and ammonia emissions from an open-freestall dairy in southern Idaho, *J. Environ. Qual.*, 42:10–20, 2013.
- Leytem, A. B., Williams, P., Zuidema, S., Martinez, A., Chong, Y. L., Vincent, A., Vincent, A., Cronan, D., Kliskey, A., Wulfhorst, J. D., Alessa, L., and Bjerneberg, D.: Cycling phosphorus and nitrogen through cropping systems in an intensive dairy production region, *Agronomy*, 11, 1005, <https://doi.org/10.3390/agronomy11051005>, 2021.
- 800 Liu, Z., Zhou, M., Chen, Y., Chen, D., Pan, Y., Song, T., Ji, D., Chen, Q., and Zhang, L.: The nonlinear response of fine particulate matter pollution to ammonia emission reductions in North China, *Environ. Res. Lett.*, 16, 034014, <https://doi.org/10.1088/1748-9326/abdf86>, 2021.
- 805 Marais, E. A., Pandey, A. K., Van Damme, M., Clarisse, L., Coheur, P.-F., Shephard, M. W., et al.: UK ammonia emissions estimated with satellite observations and GEOS-Chem. *Journal of Geophysical Research: Atmospheres*, 126, e2021JD03523 <https://doi.org/10.1029/2021JD035237>, 2021.
- 810 Müller, M., Mikoviny, T., Feil, S., Haidacher, S., Hanel, G., Hartungen, E., et al.: A compact PTR-ToF-MS instrument for airborne measurements of volatile organic compounds at high spatiotemporal resolution, *Atmospheric Measurement Techniques*, 7(11), 3763–3772. <https://doi.org/10.5194/amt-7-3763-2014>, 2014.
- 815 Nowak, J. B., Neuman, J. A., Bahreini, R., Brock, C. A., Middlebrook, A. M., Wollny, A. G., Holloway, J. S., Peischl, J., Ryerson, T. B., Fehsenfeld, F. C.: Airborne observations of ammonia and ammonium nitrate formation over Houston, Texas, *J. Geophys. Res.*, 115(22), D22304, <https://doi.org/10.1029/2010JD014195>, 2010.
- Nowak, J. B., Neuman, J. A., Bahreini, R., Middlebrook, A. M., Holloway, J. S., McKeen, S. A.: Ammonia sources in the California South Coast Air Basin and their impact on ammonium nitrate formation, *Geophys. Res. Lett.*, 39(7), 2012.
- 820 Paulot, F., and Jacob, D. J.: Hidden cost of US agricultural exports: particulate matter from ammonia emissions, *Environ. Sci. Tech.*, 48 (2), 903–908, 2014.
- Paulot, F., Jacob, D. J., and Henze, D. K.: Sources and processes contributing to nitrogen deposition: an adjoint model analysis applied to biodiversity hotspots worldwide, *Environ. Sci. Tech.*, 47(7), 3226–3233, 2013.
- 825 Pollack, I. B., Lindaas, J., Roscioli, J. R., Agnese, M., Permar, W., Hu, L., and Fischer, E. V.: Evaluation of ambient ammonia measurements from a research aircraft using a closed-path QC-TILDAS operated with active continuous passivation, *Atmos. Meas. Tech.*, 12, 3717–3742, <https://doi.org/10.5194/amt-12-3717-2019>, 2019.
- 830 Puchalski, M.A., Rogers, C.M., Baumgardner, R., Mishoe, K.P., Price, G., Smith, M.J., Watkins, N., and Lehmann, C.M.: A statistical comparison of active and passive ammonia measurements collected at Clean Air Status and Trends Network (CASTNET) sites, *Environmental Science: Processes & Impacts*, 17, 358–369, <http://dx.doi.org/10.1039/C4EM00531G>, 2015.



- 835 Pope, C., III; Ezzati, M.; Dockery, D. W.: Fine-particulate air pollution and life expectancy in the United States, *N. Engl. J. Med.*, 360, 376–386, 2009.
- Rodgers, C. D.: *Inverse Methods for Atmospheric Sounding, Theory and Practice*, World Scientific Publishing, London, 2000.
- Rodgers, C. D., and Connor, B. J.: Intercomparison of remote sounding instruments, *J. Geophys. Res.*, 108, 4116, <https://doi.org/10.1029/2002jd002299>, 2003.
- 840 Roscioli, J. R., Zahniser, M. S., Nelson, D. D., Herndon, S. C., and Kolb, C. E.: New approaches to measuring sticky molecules: improvement of instrumental response times using active passivation, *J. Phys. Chem. A*, 120, 1347–1357, <https://doi.org/10.1021/acs.jpca.5b04395>, 2016.
- 845 Shephard, M. W., Cady-Pereira, K. E., Luo, M., Henze, D. K., Pinder, R. W., Walker, J. T., Rinsland, C. P., Bash, J. O., Zhu, L., Payne, V., and Clarisse, L.: TES ammonia retrieval strategy and global observations of the spatial and seasonal variability of ammonia, *Atmos. Chem. Phys.*, 11, 10743–10763, <https://doi.org/10.5194/acp-11-10743-2011>, 2011.
- 850 Shephard, M. W., McLinden, C. A., Cady-Pereira, K. E., Luo, M., Moussa, S. G., Leithead, A., Liggio, J., Staebler, R. M., Akingunola, A., Makar, P., Lehr, P., Zhang, J., Henze, D. K., Millet, D. B., Bash, J. O., Zhu, L., Wells, K. C., Capps, S. L., Chaliyakunnel, S., Gordon, M., Hayden, K., Brook, J. R., Wolde, M., and Li, S.-M.: Tropospheric Emission Spectrometer (TES) satellite observations of ammonia, methanol, formic acid, and carbon monoxide over the Canadian oil sands: validation and model evaluation, *Atmos. Meas. Tech.*, 8, 5189–5211, <https://doi.org/10.5194/amt-8-5189-2015>, 2015.
- 855 Shephard, M. W., and Cady-Pereira, K. E.: Cross-track Infrared Sounder (CrIS) satellite observations of tropospheric ammonia, *Atmos. Meas. Tech.*, 8, 1323–1336, <https://doi.org/10.5194/amt-8-1323-2015>, 2015.
- 860 Shephard, M. W., Dammers, E., Cady-Pereira, K. E., Kharol, S. K., Thompson, J., Gainariu-Matz, Y., Zhang, J., McLinden, C. A., Kovachik, A., Moran, M. and Bittman, S.: Ammonia measurements from space with the Cross-track Infrared Sounder: characteristics and applications., *Atmos. Chem. Phys.* 20(4), 2277–2302, 2020.
- Skjøth, C. A., and Geels, C.: The effect of climate and climate change on ammonia emissions in Europe, *Atmos. Chem. Phys.*, 13, 117–128, <https://doi.org/10.5194/acp-13-117-2013>, 2013.
- 865 Sun, K., Cady-Pereira, K. E., Miller, D. J., Tao, L., Zondlo, M. A., Nowak, J. B., Neuman, A., Mikoviny, T., Mueller, M., Wisthaler, A., Scarino, A. J., and Hostetler, C. A.: Validation of TES ammonia observations at the single pixel scale in the San Joaquin Valley during DISCOVER-AQ, *J. Geophys. Res.-Atmos.*, 120, <https://doi.org/10.1002/2014JD022846>, 2015.
- 870 Sun, K., Tao, L., Miller, D. J., Pan, D., Golston, L. M., Zondlo, M. A., Griffin, R. J., Wallace, H. W., Leong, Y. J., Yang, M. M., Zhang, Y., Mauzerall, D. L., Zhu, T.: Vehicle emissions as an important urban ammonia source in the United States and China, *Environ. Sci. Tech.*, 51(4), 2472–2481, <https://doi.org/10.1021/acs.est.6b02805>, 2017.
- 875 Sun, K., Zhu, L., Cady-Pereira, K., Chan Miller, C., Chance, K., Clarisse, L., Coheur, P.-F., González Abad, G., Huang, G., Liu, X., Van Damme, M., Yang, K., and Zondlo, M.: A physics-based approach to oversample multi-satellite, multispecies observations to a common grid, *Atmos. Meas. Tech.*, 11, 6679–6701, <https://doi.org/10.5194/amt-11-6679-2018>, 2018.



- Susskind, J., Barnet, C. D., and Blaisdell, J. M.: Retrieval of atmospheric and surface parameters from AIRS/AMSU/HSB data in the presence of clouds, *IEEE T. Geosci. Remote*, 41, 390–409, 2003.
- 880 Sutton, M. A., Reis, S., Riddick, S. N., Dragosits, U., Nemitz, E., Theobald, M. R., Tang, Y. S., Braban, C. F., Vieno, M., Dore, A. J., Mitchell, R. F., Wanless, S., Daunt, F., Fowler, D., Blackall, T. D., Milford, C., Flechard, C. R., Loubet, B., Massad, R., Cellier, P., Personne, E., Coheur, P. F., Clarisse, L., Van Damme, M., Ngadi, Y., Clerbaux, C., Skjøth, C. A., Geels, C., Hertel, O., Wichink Kruit, R. J., Pinder, R. W., Bash, J. O., Walker, J. T., Simpson, D.,
- 885 Horváth, L., Misselbrook, T. H., Blecker, A., Dentener, F., and de Vries, W.: Towards a climate-dependent paradigm of ammonia emission and deposition, *Philos. Trans. R. Soc. Lond. B. Biol. Sci.*, 368(1621), 20130166, <https://doi.org/10.1098/rstb.2013.0166>, 2013.
- Van Damme, M., Erisman, J. W., Clarisse, L., Dammers, E., Whitburn, S., Clerbaux, C., Dolman, A. J., and Coheur, P. F.: Worldwide spatiotemporal atmospheric ammonia (NH₃)
- 890 columns variability revealed by satellite, *Geophys. Res. Lett.*, 42(20), 8660–8668, <https://doi.org/10.1002/2015GL065496>, 2015.
- Van Damme, M., Clarisse, L., Whitburn, S., Hadji-Lazaro, J., Hurtmans, D., Clerbaux, C., Coheur P.: Industrial and agricultural ammonia point sources exposed, *Nature*, 564, 99–103, <https://doi.org/10.1038/s41586-018-0747-1>, 2018.
- 895 Wang, R., Guo, X., Pan, D., Kelly, J. T., Bash, J. O., Sun, K., et al., Monthly patterns of ammonia over the contiguous United States at 2-km resolution. *Geophysical Research Letters*, 48, e2020GL090579. <https://doi.org/10.1029/2020GL090579>, 2021.
- Warner, J. X., Wei, Z., Strow, L. L., Dickerson, R. R., and Nowak, J. B.: The global tropospheric ammonia distribution as seen in the 13-year AIRS measurement record, *Atmos. Chem. Phys.*,
- 900 16, 5467–5479, <https://doi.org/10.5194/acp-16-5467-2016>, 2016.
- Warner, J. X., Dickerson, R. W., Wei, Z., Strow, L. L., Wang, Y., and Liang, Q.: Increased atmospheric ammonia over the world’s major agricultural areas detected from space, *Geophys. Res. Lett.*, 44, <https://doi.org/10.1002/2016GL072305>, 2017.
- Whitburn, S., Van Damme, M., Kaiser, J. W., van der Werf, G. R., Turquety, S., Hurtmans, D., Clarisse, L., Clerbaux, C., and Coheur, P. F.: Ammonia emissions in tropical biomass burning regions: Comparison between satellite-derived emissions and bottom up_re inventories, *Atmos. Environ.*, 121, 42–854, 2015.
- 905 Whitburn, S., Van Damme, M., Clarisse, L., Turquety, S., Clerbaux, C., and Coheur, P.-F.: Doubling of annual ammonia emissions from the peat fires in Indonesia during the 2015 El Niño, *Geophys. Res. Lett.*, 43, 2016GL070,620, 2016.
- 910 Worden, J., Bowman, K., Noone, D., Beer, R., Clough, S., Eldering, A., Fisher, B., Goldman, A., Gunson, M., Herman, R., Kulawik, S., Lampel, M., Luo, M., Osterman, G., Rinsland, C., Rodgers, C., Sander, S., Shephard, M., and Worden, H.: Tropospheric Emission Spectrometer observations of the tropospheric HDO/H₂O ratio: Estimation approach and characterization, *J. Geophys. Res.*, 111, D16309, <https://doi.org/10.1029/2005JD006606>, 2006.
- 915 Xu, P., Liao, Y. J., Lin, Y. H., Zhao, C. X., Yan, C. H., Cao, M. N., Wang, G. S., and Luan, S. J.: High-resolution inventory of ammonia emissions from agricultural fertilizer in China from 1978 to 2008, *Atmos. Chem. Phys.*, 16, 1207–1218, <https://doi.org/10.5194/acp-16-1207-2016>, 2016.



- 920 Zavyalov, V., Esplin, D., Scott, D., Esplin, B., Bingham, G., Hoffman, E., Lietzke, C., Predina, J., Frain, R., Suwinski, L., Han, Y., Major, C., Graham, B., Phillips, L.: Noise performance of the CrIS instrument, *J. Geophys. Res.-Atmos.*, 118, 13,108–13,120, <https://doi.org/10.1002/2013JD020457>, 2013.
- 925 Zhu, L., Henze, D. K., Cady-Pereira, K. E., Shephard, M. W., Luo, M., Pinder, R. W., Bash, J. O., and Jeong, G.-R.: Constraining U.S. ammonia emissions using TES remote sensing observations and the GEOS-Chem adjoint model, *J. Geophys. Res.-Atmos.*, 118, <https://doi.org/10.1002/jgrd.50166>, 2013.